ELSEVIER

Journal of Nuclear Materials 313–316 (2003) 388–392

journal of nuclear materials

www.elsevier.com/locate/jnucmat

Material erosion at the vessel walls of future fusion devices

R. Behrisch [a,*], G. Federici [b], A. Kukushkin [b], D. Reiter [c]

[a] *Max Planck Institut für Plasmaphysik, Euratom Association, Boltzmanstrasse 2, D-85748 Garching, Germany*
[b] *ITER Garching Joint Work Site, Boltzmannstraße 2, D-85748 Garching, Germany*
[c] *Institut für Plasmaphysik Forschungszentrum Jülich, D-52425 Jülich, Germany*

Received 27 May 2002; accepted 12 October 2002

Abstract

For a next-step fusion device the erosion at the vessel walls during normal operation caused by the bombardment with different species from the plasma is estimated. The wall fluxes are calculated for a given 'burning' plasma with the computer code B2-EIRENE. With the known sputtering yields the erosion rates for vessel walls made out of Be, C, Fe, Mo or W, are calculated. The erosion by ions is found to be of the same order of magnitude as the erosion by energetic neutrals. The erosion has minima around the area of gas feed and maxima close by and at the bottom near the baffles of the divertor. The calculated total erosion is of the order of 10^{21} to 10^{22} atom/s for low Z materials, and a factor 10–20 lower for high Z materials, such as W, resulting in about 5 kg per full-day of operation or 1 t/y.

PACS: 28.52.Fa; 52.40.H; 52.55.Fa; 81.05.T; 81.65.C
Keywords: Sputtering; Beryllium; Tungsten; Carbon; Tokamaks

1. Introduction

One very critical problem for next-step fusion devices (e.g., ITER) and for a future fusion reactor is the erosion at the plasma-facing areas of the vessel walls, especially by sputtering due to bombardment with energetic ions and neutrals from the plasma. For a continuously burning plasma the particle confinement must be limited in order to ensure exhaust of the ^{4}He ash [1,2]. These losses from the plasma are the cause of plasma wall interactions, leading to erosion, i.e. thinning of the wall material, the introduction of impurities into the plasma boundary and core, and the accumulation of tritium in the vessel walls due to implantation and co-deposition, i.e. re-deposition of the eroded atoms at remote colder vessel wall areas and co-implantation with hydrogen isotopes (i.e. tritium).

In order to get reasonable values for the erosion of different wall materials, consistent with the operational scenario, the fluxes, energy and angular distributions of charge-exchange neutrals and of ions from an ignited plasma to the vessel walls have been calculated for ITER-FEAT [3,4] using the B2-EIRENE code [5–7]. With the known sputtering yield data for Be, C, Fe, Cu, Mo or W [8–14], the total erosion at the vessel walls was calculated.

2. Calculation of the wall fluxes

The ignited plasma in ITER has a flat density profile in the core of $n_e \approx 10^{20}$ m^{-3} with a sharp decrease toward the separatrix position. The plasma temperatures are peaked, with central ion and electron temperatures of $T_i \approx 23$ keV and $T_e \approx 30$ keV [4]. The parameters of the background edge plasma are calculated with the B2-Eirene code (carbon target, 100 MW power entering the

* Corresponding author. Tel.: +49-89 3299 1250/3291 2554; fax: +49-89 3299 1212/3299 1149.
E-mail address: reb@ipp-garching.mpg.de (R. Behrisch).

0022-3115/03/$ - see front matter
PII: S0022-3115(02)01580-5

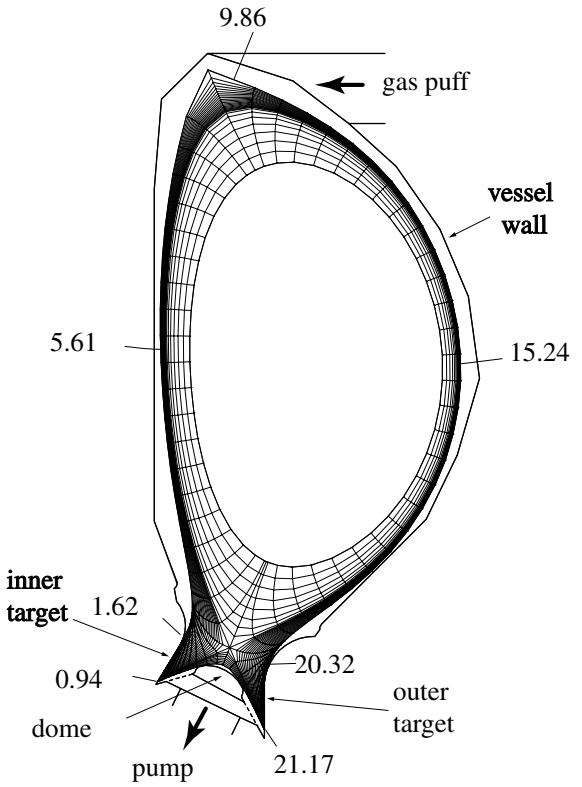

Fig. 1. Model geometry with the grid expanded to 80% of the poloidal magnetic flux. Several values of the reference distance (m) along the grid edge, which is used for plotting the profiles below, are also shown.

scrape-off layer, peak power loading ~9 MW/m^2) [15], assuming walls saturated with the hydrogen isotopes. To compensate for the particles pumped by the divertor, gas is fed in at the top of the torus, Fig. 1.

The charge-exchange neutral fluxes are calculated following the approach of [16]. A special non-random treatment is used in a combination with the Monte-Carlo method in a stand-alone Eirene run using the plasma background from the B2-Eirene calculations (modified in the core as described below). In this approach, the neutral densities in the grid cells and fluxes onto the surfaces are first calculated in a usual Monte-Carlo way. Then the neutral fluxes resulting from charge-exchange with the background plasma ions, together with those originating directly from the wall reflection, are evaluated along the specified chords for a set of the neutral energy values, using the calculated neutral densities and incident fluxes for the neutral sources. With a proper selection of the viewing chords (29 chords viewing at different angles at each wall location), this approach allows to achieve a desirable resolution simultaneously in the particle energy, in the incidence angle, and in the co-ordinate along the grid edge. The obtained neutral spectra integrated with proper weights over the particle energy and incidence angles (both polar and azimuthal) yield the profiles of the neutral fluxes, the neutral mean energy, and the erosion along the chamber wall. This method ensures much better statistical precision than a direct Monte-Carlo evaluation of the neutral spectra [17].

The accuracy of these spectra depends also on how much of the core plasma is included. Taking only a narrow stripe of the core plasma just inside the separatrix is insufficient, because the core plasma constitutes the major source of the high-energy neutrals. In the calculations reported here, the core part of the grid is expanded inwards, as shown in Fig. 1, from ~95% of the poloidal magnetic flux as used in B2-Eirene calculations [15] to ~80% of the flux, and the core plasma profiles are specified there, corresponding to the ITER operational scenario [4]. The plasma temperature at the innermost flux surface is then about 4 keV, so that the neutral energy range below 5 keV is treated reasonably well.

3. Particle fluxes and energies

The energy spectra of the incident neutrals are calculated in a four-dimensional phase space (energy, location, incidence angle, azimuthal angle). These spectra are illustrated in Figs. 2 and 3, where different moments of the distribution function and different cross-sections of the phase space are shown. Fig. 2 shows the profile along the wall of the total (i.e. integrated over the energy and incidence angles) flux of neutrals and their average energy. Fig. 3(a) shows the energy spectra of charge-exchange neutrals leaving the plasma along the normal to the surface at different locations indicated in Fig. 1. The angular distribution of the neutrals with energy of 500 eV at two different locations is presented in Fig. 3(b). Viewing chords lying in the radial plane are used

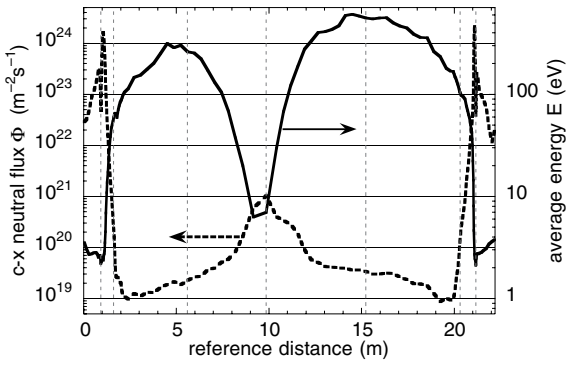

Fig. 2. Calculated profile of the total flux of charge-exchange neutrals and of their mean energy along the grid edge. Sharp peaks of the flux correspond to the target areas. The locations indicated in Fig. 1 are marked with vertical lines.

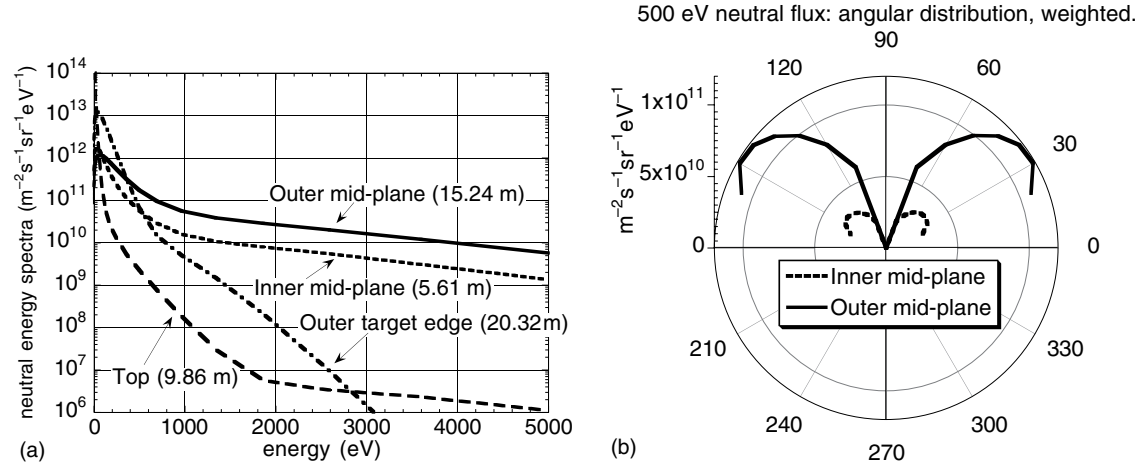

Fig. 3. (a) Calculated energy distributions of the charge-exchange neutrals leaving the plasma normal to the surface at different locations. (b) Calculated angular distribution of the energetic (500 eV) neutrals hitting the outer and inner vessel wall in the midplane. The calculated fluxes are corrected for the opening angle and the angle between the incident flux and the wall area (a factor $|\sin\alpha\cos\alpha|$, where α is the angle of the neutral velocity vector to the wall).

for this scan. The data in Fig. 3(b) are weighted with $|\sin\alpha\cos\alpha|$, where α is the angle of the neutral velocity vector to the wall. This weighting makes visible the relative contribution of particles with different incidence angles to the total particle flux.

Since the plasma parameters are only determined on the computational grid, Fig. 1, some assumptions have to be taken for the region between the outer edge of the grid and the real wall in order to evaluate the effect of wall sputtering by plasma ions (the hydrogen isotopes, He^{+} and He^{++} as well as the impurity ions in the scrape-off layer plasma). We assume here that the radial ion fluxes continue unchanged to the wall, and the electron and ion temperatures decay exponentially with 3 cm fall-off

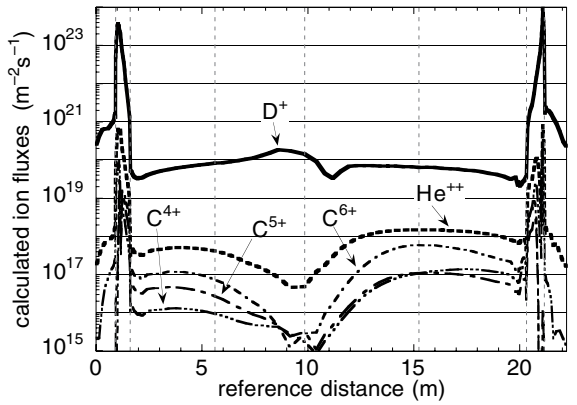

Fig. 4. Calculated profiles of the total flux of the various ions onto the vessel walls. Sharp peaks of the fluxes correspond to the target areas.

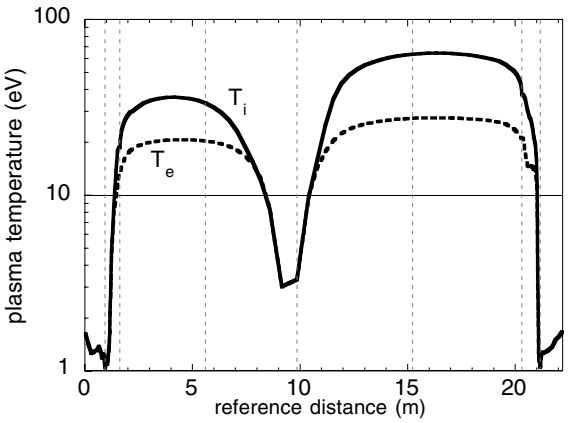

Fig. 5. Profiles of ion (T_i) and electron (T_e) temperatures along the outer grid edge.

length until they reach 10 eV and stay constant at this level further out. These temperatures are used to evaluate the energy of the ions bombarding the wall, assuming the Maxwellian distribution with ion temperature, shifted by the sheath potential calculated from the electron temperature [18]. The distribution of the ion fluxes and the plasma temperatures along the outer edge of the grid is shown in Figs. 4 and 5.

4. Erosion at different wall areas

The poloidal distribution of the erosion at the vessel walls for different materials calculated for the particle fluxes and the sputtering yields are shown in Fig. 6.

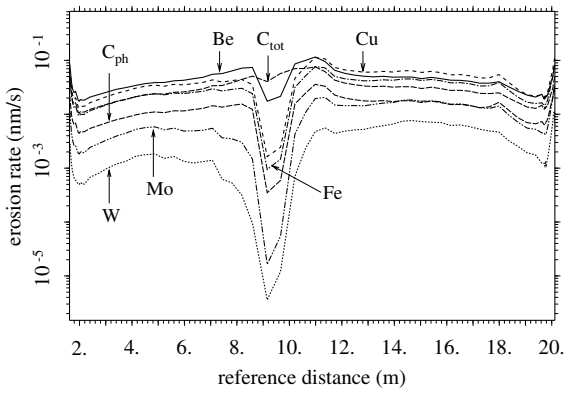

Fig. 6. Poloidal distribution of the erosion by sputtering for different materials at the outer mid plane of the vessel walls of ITER FEAT.

The increase of sputtering at oblique angles of incidence is also taken into account, resulting in sputtering yields increased by about a factor of 2 compared to normal incidence. There are erosion minima at the top close to the gas inlet, due to plasma cooling, accompanied by maxima close by (except for carbon due to the chemical erosion).

The integrated gross erosion, i.e. neglecting re-deposition, due to ions and the energetic neutrals is plotted for the different wall materials in Fig. 7(a), while (b) shows the upper estimate for the time of continuous operation until 5 mm of wall material are eroded by sputtering at the areas of maximum erosion, i.e. at the reference distance of about 11 m. The real lifetime could be an order of magnitude longer due to re-deposition of the sputtered material in the erosion areas.

5. Discussion

In calculating the wall fluxes with B2-Eirene, several approximations had to be made, such as details of the geometry, resulting in uncertainties. In the calculations a carbon wall was taken, however a test has shown, that the fluxes increased by less than 20% for a tungsten wall. Due to the neutrals and ions impinging onto the vessel walls at low energy, the sputtering yields at energies close to the threshold energy are critical. However here the yields have the largest uncertainties, which depend also on the surface topography and impurities on the surface. Some of the material may be re-deposited and removed several times. This means that the numbers given here are upper limits. However, other erosion mechanisms, such as evaporation, flaking and arcing [20] are not included.

There is considerable gross erosion by sputtering for all materials. The contributions of ions and neutrals from the plasma to this erosion are of the same order of magnitude. The integrated total erosion due to ions and the energetic neutrals for the different wall materials (Fig. 7(a)) shows that due to the larger sputtering yields for the low Z materials, the number of atoms eroded for these materials is a factor of 10–20 larger compared to high Z materials, such as W. However the total mass loss is similar for all materials making up to several kg per day or about one ton per year.

The maximum wall thinning for the low Z materials is about 3.5 mm/y, while for high Z materials, such as W, it is 0.22 mm/y, i.e. about a factor of 15 lower. These values are in reasonable agreement with erosion measurements at the JET vessel walls [19]. With respect to wall thinning, W is favourable for the use at the vessel walls because it has the longest 'erosion lifetime' (Fig. 7(b)). With respect to plasma contamination, the probability of the eroded atoms entering into the plasma core, their lifetime in the plasma core and the tolerable concentration of these ions in a burning fusion plasma have to be taken into account [20]. The tolerable concentration of W in the plasma is nearly three orders of magnitude lower than for low Z atoms, such as Be and C. However, recent observations have shown, that W

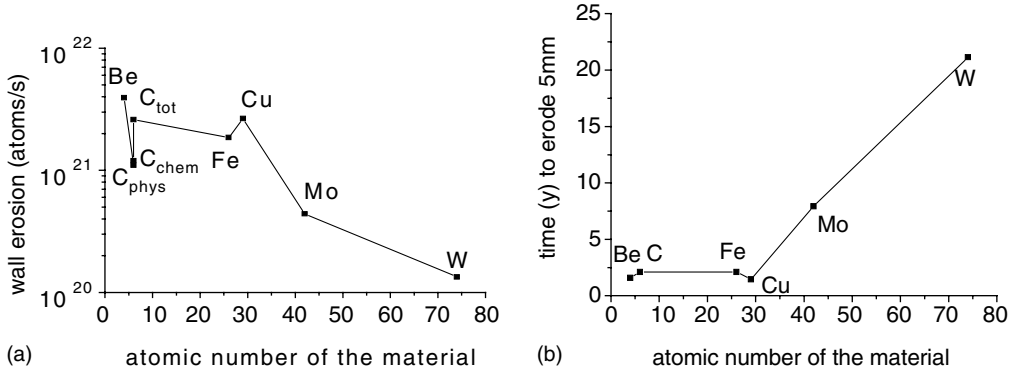

Fig. 7. (a) Integrated gross erosion due to ions and the energetic neutrals. (b) Upper estimate for the time until a thickness of 5 mm is eroded by sputtering at the area of largest erosion, i.e. at the reference distance of about 11 m.

can be effectively removed from the plasma centre by central heating [21,22]. Since this central heating is natural for burning plasmas, also from the viewpoint of plasma contamination W may be a possible plasma facing material. The ion and neutral flux densities to the vessel walls are of the order of 10^{20} $m^{-2}\,s^{-1}$ which may be critical with respect to the T implantation and accumulation in the vessel walls.

6. Summary and conclusions

The numbers calculated here for the wall erosion for different materials and for the different wall areas show minima around the area of gas feed and maxima close by and at the bottom near the divertor plates. The total erosion corresponds for all materials to an amount of the order of kg per full-day or one t per year of continuous operation. Both ions and energetic charge-exchange neutrals contribute to the erosion. While this erosion rate for low- and medium-Z materials is acceptable for a low duty-factor operation device, such as ITER, it will reduce the erosion lifetime for a reactor unless it can be compensated by simultaneous re-deposition at the areas of a large erosion. The wall erosion is also of concern in respect to the build-up of the critical impurity concentration in a burning fusion plasma.

References

[1] R. Behrisch, V. Prozesky, Nucl. Fusion 30 (1990) 2141.
[2] D. Reiter, G.H. Wolf, H. Kever, Nucl. Fusion 30 (1990) 2141.
[3] G. Federici, J.N. Brooks, D.P. Coster, et al., J. Nucl. Mater. 290–293 (2001) 260.
[4] Technical Basis for ITER FEAT outline design, ITER EDA Documentation, Series No 9, IAEA, Vienna, 2000.
[5] D. Reiter, J. Nucl. Mater. 196–198 (1992) 80.
[6] D. Reiter, H. Kever, G.H. Wolf, et al., Plasma Phys. Controll. Fusion 33 (1991) 1579.
[7] R. Schneider, D. Reiter, H.-P. Zehrfeld, et al., J. Nucl. Mater. 196–198 (1992).
[8] W. Eckstein, C. García-Rosales, J. Roth, W. Ottenberger, Max-Planck Institut für Plasmaphysik, Garching, Report IPP 9/82, 1993, and private communication.
[9] C. García-Rosales, W. Eckstein, J. Roth, J. Nucl. Mater. 218 (1994) 8.
[10] C. García-Rosales, J. Roth, in: E. Joffrin, P. Platz, P.E. Stott (Eds.), 21st EPS Conference on Controlled Fusion and Plasma Physics, Montpellier, 18B II, 1994, p.770.
[11] J. Roth, C. García-Rosales, Nucl. Fusion 36 (1996) 1647.
[12] J. Roth, J. Nucl. Mater. 266–269 (1999) 51.
[13] R.K. Janev (Ed.), Atomic and Plasma-Material Interaction Data for Fusion, Part A, vol. 7, IAEA, Vienna, 1998.
[14] R.E.H. Clark (Ed.), Atomic and Plasma-Material Interaction Data for Fusion, Part B, vol. 7, IAEA, Vienna, 2001.
[15] H.D. Pacher, A.S. Kukushkin, G.W. Pacher, G. Janeschitz, these Proceedings.
[16] H. Verbeek, J. Stober, D.P. Coster, et al., Nucl. Fusion 38 (1998) 1789.
[17] H.M. Hughes, D. Post, J. Comp. Phys. 28 (1978) 43.
[18] P. Stangeby, in: D.E. Post, R. Behrisch (Eds.), NATO ASI series, Plenum, New York and London, 1984, p. 34.
[19] M. Mayer, R. Behrisch, K. Plamann, P. Andrew, J.P. Coad, A.T. Peacock, J. Nucl. Mater. 266–269 (1999) 604.
[20] R. Behrisch, Proc 8th PET workshop, Helsinki, 2001, Contributions to Plasmaphysics 42 (2002) 431.
[21] R. Dux, R. Neu, et al., these Proceedings. PII: S0022-3115(02)01508-8.
[22] R. Neu et al., these Proceedings. PII: S0022-3115(02)01386-7.